colorants

MDPI

Article

Synthesis of High Near-Infrared Reflective Black Pigment Based on YMn_2O_5

Kazuki Yamaguchi, Satoru Mochizuki, Yudai Nagato, Takuro Morimoto and Toshiyuki Masui *

Department of Chemistry and Biotechnology, Faculty of Engineering, and Center for Research on Green Sustainable Chemistry, Tottori University, 4-101, Koyama-cho Minami, Tottori 680-8552, Japan; yamaguchi@tottori-u.ac.jp (K.Y.); m23j5031b@edu.tottori-u.ac.jp (S.M.); b18t3063c@gmail.com (Y.N.); m21j5037h@gmail.com (T.M.)

* Correspondence: masui@tottori-u.ac.jp; Tel.: +81-857-31-5264

Abstract: $Y(Mn_{0.95}M_{0.05})_2O_5$ (M = Al, Fe, Ga, Ti, and Zr) samples were synthesized via a sol–gel method using citric acid to find a new near-infrared (NIR) reflective black pigment. Among these samples, the optical reflectance of $Y(Mn_{0.95}Fe_{0.05})_2O_5$ and $Y(Mn_{0.95}Ga_{0.05})_2O_5$ in the near-infrared region was found to be larger than that of YMn_2O_5. Then, the concentration of the dopant (Fe or Ga) was changed between 0 and 15%, and the resulting UV–Vis–NIR reflectance spectra were measured. As a result, the optical reflectance of the Fe-doped samples decreased in the near-infrared region, while that of the Ga-doped samples increased. Accordingly, $Y(Mn_{1-x}Ga_x)_2O_5$ ($0 \leq x \leq 0.20$) samples were synthesized, and the crystal structure, particle size, optical properties, and color of the samples were characterized. The single-phase samples were obtained in the composition range of $0 \leq x \leq 0.15$, and the lattice volume decreased with increasing Ga^{3+} concentration. Optical absorption below 850 nm was attributed to the charge transfer transition between O_{2p} and Mn_{3d} orbitals, and the absorption wavelength of $Y(Mn_{1-x}Ga_x)_2O_5$ shifted to the shorter wavelength side as the Ga^{3+} content increased, because of the decrease in the Mn^{3+} concentration. Although the sample color became slightly reddish black by the Ga^{3+} doping, the solar reflectance in the near-infrared region reached 47.6% at the composition of $Y(Mn_{0.85}Ga_{0.15})_2O_5$. Furthermore, this NIR reflectance value was higher than those of the commercially available products ($R < 45\%$).

Keywords: black pigment; environmentally friendly; Mn^{4+} ion; yttrium manganate

check for updates

Citation: Yamaguchi, K.; Mochizuki, S.; Nagato, Y.; Morimoto, T.; Masui, T. Synthesis of High Near-Infrared Reflective Black Pigment Based on YMn_2O_5. *Colorants* **2023**, *2*, 705–715. https://doi.org/10.3390/colorants2040036

Academic Editor: Anthony Harriman

Received: 14 September 2023
Revised: 2 November 2023
Accepted: 30 November 2023
Published: 6 December 2023

Copyright: © 2023 by the authors. Licensee MDPI, Basel, Switzerland. This article is an open access article distributed under the terms and conditions of the Creative Commons Attribution (CC BY) license (https://creativecommons.org/licenses/by/4.0/).

1. Introduction

As the need for power and energy conservation increases, there is a growing demand for thermal barrier coatings. A black color, in particular, usually causes a large rise in room temperature and requires a large amount of cooling energy when it is applied to roofing materials and automobiles. Therefore, black thermal barrier pigments with high performance are required. Existing black thermal barrier inorganic pigments such as iron titanate (Fe_2TiO_4) and iron–chromium mixed oxide ($(Fe,Cr)_2O_3$) have typically been used so far [1]. However, these materials are not pure black, and their solar reflectance is not sufficient. Furthermore, safety considerations have recently led to a demand for chromium-free materials, and new black thermal barrier materials are needed to replace existing materials [2–5].

Based on this situation, we focused on YMn_2O_5 as a base material with the aim of developing a novel environmentally friendly black heat-blocking pigment. YMn_2O_5 adopts an orthorhombic structure (space group: *Pbam*), where Mn^{3+} and Mn^{4+} ions are anti-ferromagnetically ordered; the former are coordinated with five O^{2-} ions and the latter are six coordinated [6,7]. Although this compound has been reported as a catalyst [8,9] and a ferroelectric material [10,11], there have been few studies on its color and optical properties. $YMnO_3$, which is composed of the same metallic elements but has a different composition, is already known as a black heat-blocking pigment [12,13]. However, this

compound has a slightly bluish black color, and its solar reflectance in the wavelength range of 700–1300 nm, which is most involved in heat generation, is not so high. There are similar challenges with respect to other conventional black pigments, such as manganese–bismuth oxide and calcium–manganese–titanium oxide. Thus, the development of a black pigment with a higher solar reflectance in the wavelength range of 700–1300 nm is desired.

The band structure of YMn_2O_5 is composed of a valence band consisting of O_{2p} orbitals and a conduction band consisting of Mn_{3d} orbitals [14]. Accordingly, it is considered that YMn_2O_5 strongly absorbs visible light (300~700 nm) due to the O_{2p}–Mn_{3d} charge transfer transition and reflects near-infrared (NIR) light (700–2500 nm). In this study, we synthesized $Y(Mn_{0.95}M_{0.05})_2O_5$ (M = Al, Fe, Ga, Ti, and Zr) samples and characterized their NIR reflectance property to obtain a new environmentally friendly pigment that possesses high thermal barrier performance and a sufficient black color. Among these samples, the optical reflectance of $Y(Mn_{0.95}Fe_{0.05})_2O_5$ and $Y(Mn_{0.95}Ga_{0.05})_2O_5$ in the near-infrared region was improved compared with that of YMn_2O_5. Accordingly, $Y(Mn_{1-x}M_x)_2O_5$ (M = Fe or Ga, $0 \leq x \leq 0.15$) samples were synthesized, and it was found that Ga^{3+}-doping was more effective than Fe^{3+} in enhancing the NIR reflectivity. In this study, therefore, $Y(Mn_{1-x}Ga_x)_2O_5$ ($0 \leq x \leq 0.20$) samples were synthesized, and the crystal structure, particle size, optical properties, and color of the samples were characterized. From the viewpoint of practical application, a color comparison with $YMnO_3$ and commercially available black pigments and an evaluation of chemical stability were carried out. As a result, we found that the $Y(Mn_{0.85}Ga_{0.15})_2O_5$ pigment exhibits higher solar reflectance in the wavelength range of 700–1300 nm compared to conventional black pigments and has the potential to become a new NIR-reflective inorganic black pigment.

2. Materials and Methods

2.1. Synthesis

The $Y(Mn_{0.95}M_{0.05})_2O_5$ (M = Al, Fe, Ga, Ti, and Zr) samples were synthesized using a citrate sol–gel method. $Y(NO_3)_3{\cdot}6H_2O$ (Kishida Chemical, Osaka, Japan, 99.9%), $(CH_3COO)_2Mn{\cdot}4H_2O$ (FUJIFILM Wako Pure Chemical, Osaka, Japan, 99.9%), $Al(NO_3)_3{\cdot}9H_2O$ (FUJIFILM Wako Pure Chemical, 98.0%), $Fe(NO_3)_3{\cdot}9H_2O$ (FUJIFILM Wako Pure Chemical, 99.9%), $Ga(NO_3)_3{\cdot}8H_2O$ (Kishida Chemical, 99.0%), $[(CH_3)_2CHO]_4Ti$ (FUJIFILM Wako Pure Chemical, 95.0%), $ZrO(NO_3)_2{\cdot}2H_2O$ (FUJIFILM Wako Pure Chemical, 97.0%), and citric acid (FUJIFILM Wako Pure Chemical, 98.0%) powders were weighed as shown in Table 1. $[(CH_3)_2CHO]_4Ti$ was dissolved in a mixed solution of 5 cm^3 of deionized water, 10 cm^3 of nitric acid, and 45 cm^3 of ethanol. $ZrO(NO_3)_2{\cdot}2H_2O$ was dissolved in a mixed solution of 50 cm^3 of deionized water and 5 cm^3 of nitric acid, and the other nitrates were dissolved in 50 cm^3 of deionized water. Each raw material solution was mixed and stirred homogeneously; then, citric acid (CA) powder was added as a chelating agent. The mixed solution was stirred at 90 °C until a gel was obtained, and the gel was dried at 120 °C in an oven for 24 h. The dried gel was placed in an alumina crucible and calcined at 500 °C in air for 6 h. After calcination, the samples were again heated at 1100 °C in air for 12 h. Before characterization, the samples were ground in an agate mortar.

Table 1. Amounts of reagents used to synthesize $Y(Mn_{0.95}M_{0.05})_2O_5$ (M = Al, Fe, Ga, Ti, and Zr).

Sample	$Y(NO_3)_3{\cdot}6H_2O$	$(CH_3COO)_2Mn{\cdot}4H_2O$	Reagent of Dopant	CA
YMn_2O_5	1.3739 g	1.7582 g	—	4.1350 g
$Y(Mn_{0.95}Al_{0.05})_2O_5$	1.3879 g	1.6872 g	$Al(NO_3)_3{\cdot}9H_2O$ 0.1360 g	4.1766 g
$Y(Mn_{0.95}Fe_{0.05})_2O_5$	1.3735 g	1.6699 g	$Fe(NO_3)_3{\cdot}9H_2O$ 0.1448 g	4.1335 g
$Y(Mn_{0.95}Ga_{0.05})_2O_5$	1.3666 g	1.6617 g	$Ga(NO_3){\cdot}8H_2O$ 0.1426 g	4.1129 g
$Y(Mn_{0.95}Ti_{0.05})_2O_5$	1.3775 g	1.6746 g	$[(CH_3)_2CHO]_4Ti$ 0.1022 g	4.1455 g
$Y(Mn_{0.95}Zr_{0.05})_2O_5$	1.3564 g	1.6489 g	$ZrO(NO_3)_2{\cdot}2H_2O$ 0.0946 g	4.0819 g

The $Y(Mn_{1-x}Fe_x)_2O_5$ ($0 \leq x \leq 0.15$) and $Y(Mn_{1-x}Ga_x)_2O_5$ ($0 \leq x \leq 0.20$) samples were synthesized via the same procedure described above for the $Y(Mn_{0.95}M_{0.05})_2O_5$ (M = Fe or Ga) samples. The starting materials were weighed as listed in Tables 2 and 3.

Table 2. Amounts of reagents used to synthesize $Y(Mn_{1-x}Fe_x)_2O_5$ ($0 \leq x \leq 0.15$).

Sample	$Y(NO_3)_3 \cdot 6H_2O$	$(CH_3COO)_2Mn \cdot 4H_2O$	$Fe(NO_3)_3 \cdot 9H_2O$	CA
$Y(Mn_{0.95}Fe_{0.05})_2O_5$	1.3735 g	1.6699 g	0.1448 g	4.0973 g
$Y(Mn_{0.90}Fe_{0.10})_2O_5$	1.3729 g	1.5813 g	0.2895 g	4.1322 g
$Y(Mn_{0.85}Fe_{0.15})_2O_5$	1.3725 g	1.4930 g	0.4343 g	4.1308 g

Table 3. Amounts of reagents used to synthesize $Y(Mn_{1-x}Ga_x)_2O_5$ ($0 \leq x \leq 0.20$).

Sample	$Y(NO_3)_3 \cdot 6H_2O$	$(CH_3COO)_2Mn \cdot 4H_2O$	$Ga(NO_3) \cdot 8H_2O$	CA
$Y(Mn_{0.95}Ga_{0.05})_2O_5$	1.3666 g	1.6617 g	0.1426 g	4.1129 g
$Y(Mn_{0.90}Ga_{0.10})_2O_5$	1.3595 g	1.5658 g	0.2839 g	4.0914 g
$Y(Mn_{0.85}Ga_{0.15})_2O_5$	1.3523 g	1.4710 g	0.4236 g	4.0702 g
$Y(Mn_{0.83}Ga_{0.17})_2O_5$	1.3494 g	1.4335 g	0.4790 g	4.0616 g
$Y(Mn_{0.80}Ga_{0.20})_2O_5$	1.3452 g	1.3773 g	0.5617 g	4.0489 g

2.2. Characterization

Crystalline phases and structures were identified by means of X-ray powder diffraction (XRD; Rigaku, Ultima IV). The diffraction patterns were measured using Cu Kα radiation at 40 kV and 40 mA. The XRD data were collected by scanning in the 2θ range of 20–80°. The sampling width was 0.02°, and the scan speed was 6° min^{-1}. The lattice volumes were calculated from the XRD peak angles refined using CellCalc Ver. 2.20 software with α-Al_2O_3 as a standard. Optical reflectance spectra were recorded using an ultraviolet–visible–near-infrared (UV–Vis–NIR) spectrometer (JASCO, Hachioji, Japan, V-770 with an integrating sphere attachment) using a standard white plate as a reference. The step width was 1 nm, and the scan rate was 1000 nm min^{-1}. Electron micrographs of the sample particles were taken using a Hitachi H-7650 transmission electron microscope (TEM) operating at 100 kV. The sample particles were dispersed ultrasonically in ethanol and then supported on amorphous carbon film on a copper TEM grid. The color properties of the powder samples were evaluated in the Commission Internationale de l'Éclairage (CIE) $L^*a^*b^*C$ system using a color chromatometer (Konica-Minolta, CR-400). The L^* parameter indicates brightness or darkness on a neutral gray scale. The a^* and b^* values represent the red–green and yellow–blue axes, respectively. The chroma parameter (C) represents saturation and is calculated by the formula $C = [(a^*)^2 + (b^*)^2]^{1/2}$. The standard deviation of all values in the $L^*a^*b^*C$ color coordinate data was less than 0.1. The NIR solar reflectance (R) was calculated using the following equation [15]:

$$R = \frac{\int_{700}^{2500} r(\lambda) i(\lambda) \mathrm{d}\lambda}{\int_{700}^{2500} i(\lambda) \mathrm{d}\lambda}$$

where $r(\lambda)$ is the spectral reflectance obtained from experiments and $i(\lambda)$ is the standard solar spectrum (W m^{-2} nm^{-1}). The NIR reflectance value (R) is expressed as the integral of the product of the observed spectral reflectance and the solar irradiance divided by the product of the solar radiation, both integrated over the range of 700 to 2500 nm.

3. Results and Discussion

3.1. $Y(Mn_{0.95}M_{0.05})_2O_5$ (M = Al, Fe, Ga, Ti, and Zr)

3.1.1. X-ray Powder Diffraction (XRD)

Figure 1 shows the XRD patterns of the $Y(Mn_{0.95}M_{0.05})_2O_5$ (M = Al, Fe, Ga, Ti, and Zr) samples. In the samples with Al, Fe, Ga, and Ti, the target YMn_2O_5 phase was obtained as a single phase. On the other hand, in the sample with Zr, the target YMn_2O_5 phase

was obtained as the main phase, but $YMnO_3$ and ZrO_2 peaks were detected as impurities, resulting in a mixed phase.

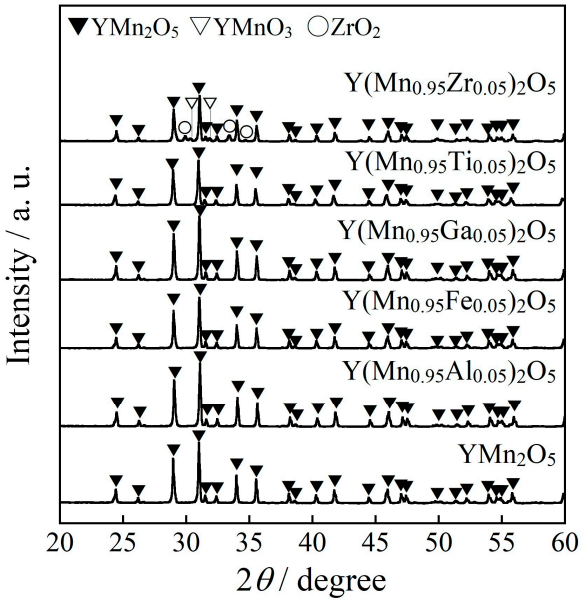

Figure 1. XRD patterns of the $Y(Mn_{0.95}M_{0.05})_2O_5$ (M = Al, Fe, Ga, Ti, and Zr) samples.

3.1.2. Ultraviolet–Visible–Near-Infrared (UV–Vis–NIR) Reflectance Spectra

The UV–Vis and NIR reflectance spectra of YMn_2O_5 and $Y(Mn_{0.95}M_{0.05})_2O_5$ (M = Al, Fe, Ga, and Ti) obtained with a single target phase in Section 3.1.1 are shown in Figure 2a,b, respectively. In the visible region, the optical absorption around 700 nm due to the O_{2p}–Mn_{3d} charge transfer transition [14] was weakened by the doping of Al, Fe, and Ga. The O_{2p}–Mn_{3d} charge transfer transition of the Mn^{3+}-doped sample was weaker than that of the host material because Mn^{3+} in the host lattice was partially replaced by Al^{3+}, Fe^{3+}, and Ga^{3+}, resulting in a lower Mn^{3+} concentration. On the other hand, the Ti^{4+}-doped sample showed enhanced optical absorption around 700 nm. The O_{2p}–Mn_{3d} charge transfer transition was not inhibited because Ti^{4+} should have replaced the Mn^{4+} sites. The ionic radius of Ti^{4+} (ionic radius at the six-coordination site: 0.0605 nm [16]) is larger than that of Mn^{4+} (ionic radius at the six-coordination site: 0.053 nm [16]), suggesting that the MnO_6 octahedron is distorted by Ti^{4+} doping. As a result, the spin-forbidden $^4A_{2g} \rightarrow {}^2E_g$, $^2T_{1g}$ transitions of Mn^{4+} were enhanced [17]. These are the reasons for the enhanced optical absorption around 700 nm due to Ti^{4+} doping.

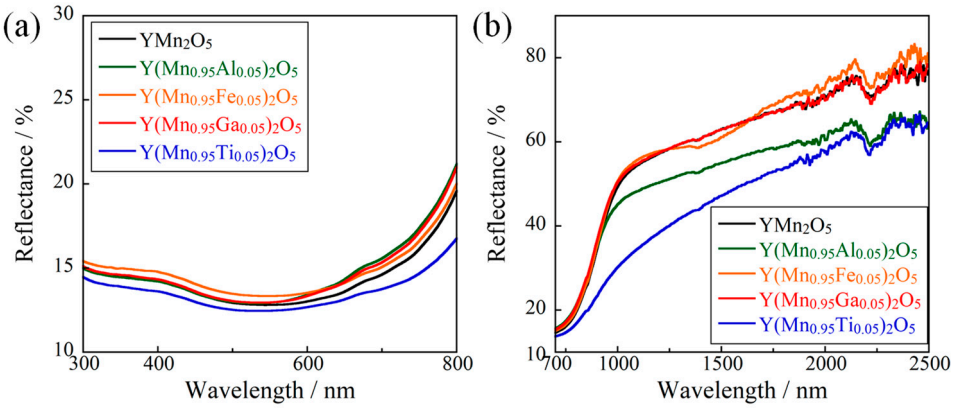

Figure 2. (**a**) UV–Vis and (**b**) NIR reflectance spectra for YMn_2O_5 and $Y(Mn_{0.95}M_{0.05})_2O_5$ (M = Al, Fe, Ga, and Ti).

In the case of M = Fe and Ga, the reflectance in the near-infrared region from 700 nm to 2500 nm was slightly improved compared to that of YMn_2O_5. This is probably due to the partial substitution of Mn^{3+} with trivalent Fe^{3+} and Ga^{3+}, which reduced the concentration of Mn^{3+} and weakened the charge transfer absorption between Mn^{3+} and Mn^{4+} [18].

On the other hand, for M = Al, the reflectance in the near-infrared region was lower than for YMn_2O_5. This is considered to be because of the ionic radius of Al^{3+} (ionic radius: 0.048 nm at five-coordination sites [16]), which distorts the crystal structure significantly and increases lattice defects. For M = Ti, the reflectance in the near-infrared region was significantly lower than that of YMn_2O_5. This is considered to be due to the partial substitution of Ti^{4+} for Mn^{4+}, which strengthens the d-d transition absorption attributed to the ^5E_g to $^5T_{2g}$ transition of Mn^{3+} [19].

3.1.3. Color Properties

The *L*a*b*C* color coordinate data and NIR solar reflectance (*R*) of the YMn_2O_5 and $Y(Mn_{0.95}M_{0.05})_2O_5$ (M = Al, Fe, Ga, and Ti) powder samples are summarized in Table 4. All the $Y(Mn_{0.95}M_{0.05})_2O_5$ samples exhibited lower *L** values than the YMn_2O_5 sample. However, the *C* value of the Al-doped sample increased, and its *R* value decreased. In the case of M = Ti, although the *C* value was lower compared to that of the host material, the *R* value also declined significantly. Only the samples with Fe or Ga additions exceeded the solar reflectance of YMn_2O_5. Thus, some Fe- or Ga-doped samples with different compositions were additionally synthesized, and their optical properties are evaluated in the next section.

Table 4. Color coordinates and NIR solar reflectance (*R*) of the YMn_2O_5 and $Y(Mn_{0.95}M_{0.05})_2O_5$ (M = Al, Fe, Ga, and Ti) powder samples.

Sample	*L**	*a**	*b**	*C*	*R*
YMn_2O_5	28.2	+2.83	−0.44	2.86	42.9
$Y(Mn_{0.95}Al_{0.05})_2O_5$	27.5	+4.95	+1.73	5.24	39.5
$Y(Mn_{0.95}Fe_{0.05})_2O_5$	25.5	+3.24	+0.10	3.24	43.5
$Y(Mn_{0.95}Ga_{0.05})_2O_5$	25.8	+3.93	+0.53	3.97	43.7
$Y(Mn_{0.95}Ti_{0.05})_2O_5$	25.2	+2.58	+0.20	2.59	31.2

3.2. $Y(Mn_{1-x}Fe_x)_2O_5$ ($0 \leq x \leq 0.15$)

Figure 3 shows the XRD patterns of the $Y(Mn_{1-x}Fe_x)_2O_5$ ($0 \leq x \leq 0.15$) samples. In the *x* range of 0 to 0.10, the YMn_2O_5 phase was obtained as a single phase. However, in the case of $x = 0.15$, the target phase and some impurities were detected. Therefore, the solid solubility limit of $Y(Mn_{1-x}Fe_x)_2O_5$ is less than 15%. Figure 4a shows the UV–visible reflectance spectra of the $Y(Mn_{1-x}Fe_x)_2O_5$ samples, where *x* is from 0 to 0.15. All samples absorbed visible light at wavelengths shorter than 700 nm, due to the O_{2p}–Mn_{3d} charge transfer transition [14]; as a result, these samples were black. However, as shown in Figure 4b, the reflectance at wavelengths of 700 nm to 2500 nm was decreased with increasing Fe^{3+} content, because of the d-d transition attributed to the $^6A_1$ to $^4T_1$ transition of Fe^{3+} [20].

The *L*a*b*C* color coordinate data and NIR solar reflectance (*R*) of the $Y(Mn_{1-x}Fe_x)_2O_5$ powder samples, where *x* is from 0 to 0.15, are summarized in Table 5. Similarly to the results in Figure 4, the NIR reflectance value decreased with increasing Fe^{3+} content. Unfortunately, we found that increasing the amount of iron doping degraded performance, so we decided to study the Ga-doped samples in detail.

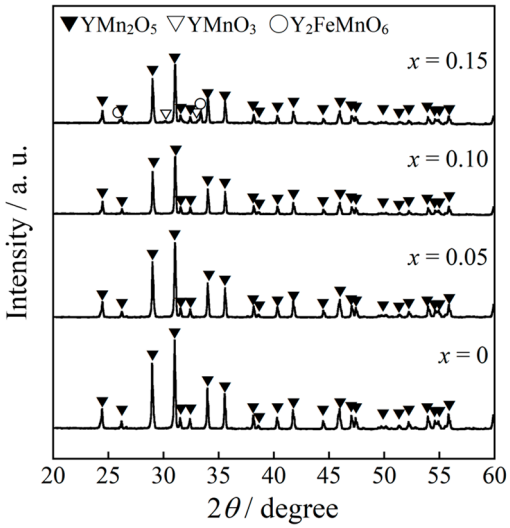

Figure 3. XRD patterns of the $Y(Mn_{1-x}Fe_x)_2O_5$ ($0 \leq x \leq 0.15$) samples.

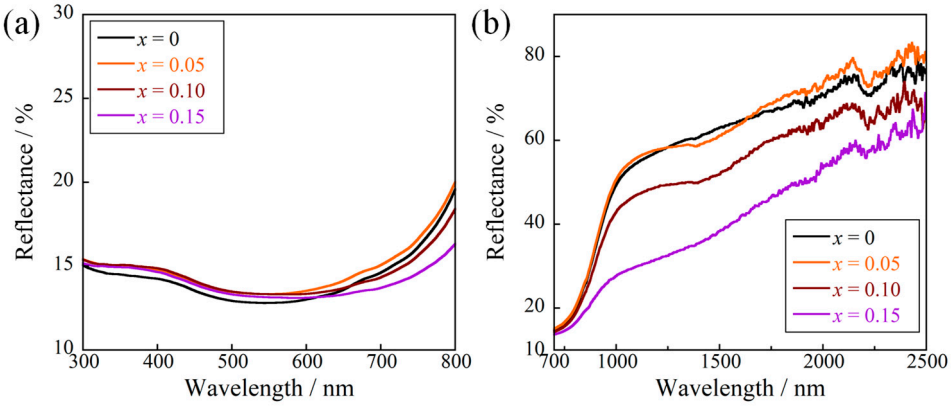

Figure 4. (**a**) UV–Vis and (**b**) NIR reflectance spectra for the $Y(Mn_{1-x}Fe_x)_2O_5$ samples, where x is from 0 to 0.15.

Table 5. Color coordinates and NIR solar reflectance (R) of the $Y(Mn_{1-x}Fe_x)_2O_5$ powder samples, where x is from 0 to 0.15.

Sample	*L**	*a**	*b**	*C*	*R*
YMn_2O_5	28.2	+2.83	−0.44	2.86	42.9
$Y(Mn_{0.95}Fe_{0.05})_2O_5$	25.3	+3.24	+0.10	3.24	43.5
$Y(Mn_{0.90}Fe_{0.10})_2O_5$	26.2	+2.07	−0.98	2.50	37.7
$Y(Mn_{0.85}Fe_{0.15})_2O_5$	24.7	+1.58	+1.02	1.88	28.1

3.3. $Y(Mn_{1-x}Ga_x)_2O_5$ ($0 \leq x \leq 0.20$)

3.3.1. X-ray Powder Diffraction (XRD)

Figure 5 shows the XRD patterns of the $Y(Mn_{1-x}Ga_x)_2O_5$ ($0 \leq x \leq 0.20$) samples. For x ranging from 0 to 0.15, the YMn_2O_5 phase was obtained as a single phase. In contrast, for $x \geq 0.17$, the target phase was observed as the main phase, but an additional impurity indexed as $Y_3Ga_5O_{12}$ was also detected. The composition dependence of the lattice volume of the samples calculated from each XRD pattern is shown in Figure 6. The introduction of small Ga^{3+} (ionic radius: 0.055 nm, five-coordination site [16]) ions into the Mn^{3+} (ionic radius: 0.058 nm, five-coordination site [16]) sites resulted in a linear increase in lattice volume with increasing Ga^{3+} content in the $x \leq 0.15$ range. The substitution of six-coordinated Mn^{4+} sites with Ga^{3+} is ruled out, because the ionic radius of hexacoordinated

Ga^{3+} (0.062 nm [16]) is larger than that of Mn^{4+} (0.053 nm [16]), so the lattice volume should increase with increasing Ga^{3+} concentration. The cell volumes at x = 0.17 and 0.20 were almost equal to that at x = 0.15. Thus, $Y(Mn_{1-x}Ga_x)_2O_5$ solid solutions were successfully synthesized in the x = 0 to 0.15 region.

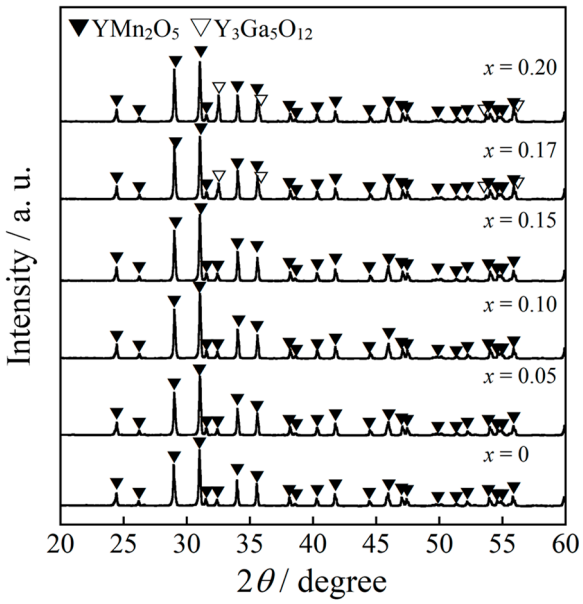

Figure 5. XRD patterns of the $Y(Mn_{1-x}Ga_x)_2O_5$ ($0 \leq x \leq 0.20$) samples.

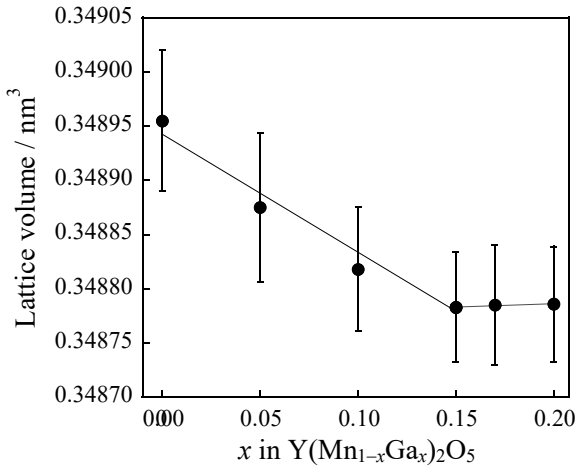

Figure 6. Compositional dependence of the lattice volume for the $Y(Mn_{1-x}Ga_x)_2O_5$ ($0 \leq x \leq 0.20$) samples.

Figure 7 shows TEM images of YMn_2O_5 and $Y(Mn_{0.85}Ga_{0.15})_2O_5$ samples obtained as a single phase. In both samples, the primary particles were very small, about 500 nm. These primary particles aggregated to form secondary particles of about 3 μm in size. No effect of Ga doping on particle size was observed. Therefore, the improvement in NIR solar reflectance due to Ga doping, which is discussed in the next section, is not due to a difference in particle size.

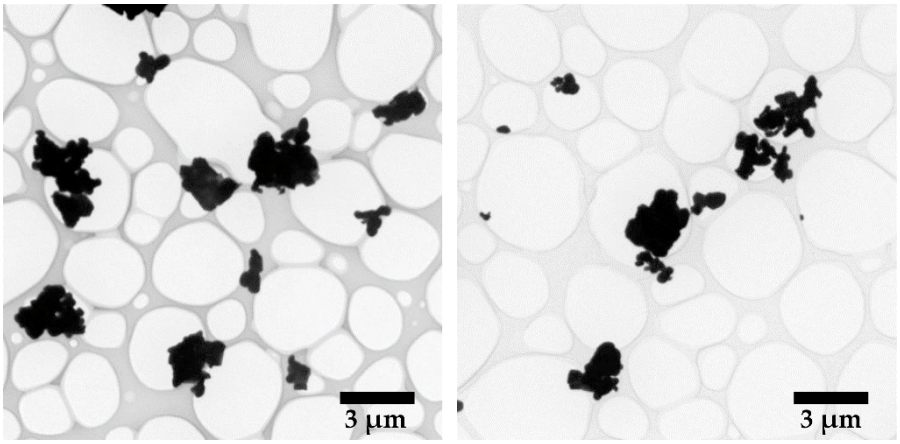

Figure 7. TEM images of the YMn_2O_5 (**left**) and $Y(Mn_{0.85}Ga_{0.15})_2O_5$ (**right**) samples.

3.3.2. Ultraviolet–Visible–Near-Infrared (UV–Vis–NIR) Reflectance Spectra

UV–visible–NIR reflectance measurements were performed for the $Y(Mn_{1-x}Ga_x)_2O_5$ ($0 \leq x \leq 0.15$) samples obtained as a single phase. The reflectance spectra in the 300–800 nm wavelength region and 700–2500 nm wavelength region are shown Figure 8a,b. All samples were found to strongly absorb visible light at wavelengths shorter than 700 nm, and this optical absorption was attributed to the O_{2p}–Mn_{3d} charge transfer transition [14]. The optical absorption was slightly weakened by the decrease in Mn concentration with increasing Ga content. Since the optical reflection in the visible light was low, these samples were black.

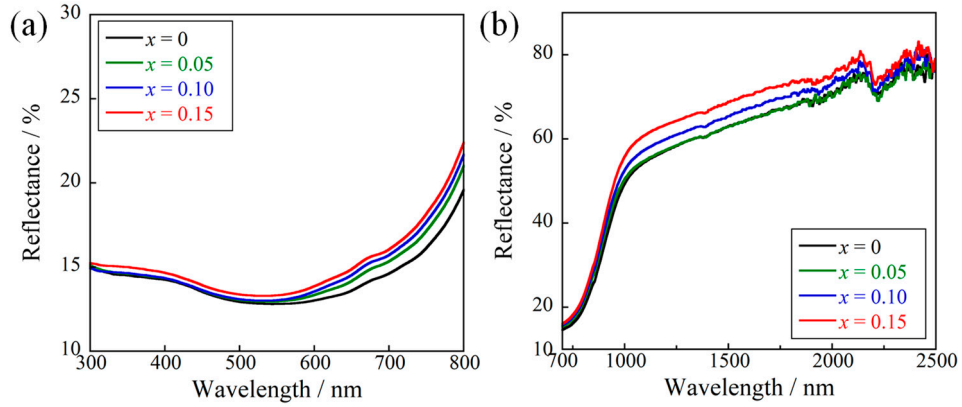

Figure 8. (**a**) UV–Vis and (**b**) NIR reflectance spectra for the $Y(Mn_{1-x}Ga_x)_2O_5$ ($0 \leq x \leq 0.15$) samples.

It was found that the reflectance at wavelengths of 700 nm to 2500 nm improved when Ga^{3+} was dissolved in YMn_2O_5. This is thought to be due to the partial substitution of Mn^{3+} with Ga^{3+}, which decreased the Mn^{3+} concentration and weakened the charge transfer transition between O_{2p} and Mn_{3d} orbitals. Furthermore, the reflectance in the near-infrared region was improved by introducing Ga^{3+}. This is probably because the reduction in the Mn^{3+} concentration also weakened the charge transfer absorption of Mn^{3+}–Mn^{4+} [16] in the near-infrared region. In the case of $x = 0.15$, the reflectance of wavelengths between 700 and 1300 nm, which is most involved in heat generation, was significantly improved.

3.3.3. Color Properties

The $L^*a^*b^*C$ color coordinate data and NIR solar reflectance (R) of the $Y(Mn_{1-x}Ga_x)_2O_5$ ($0 \leq x \leq 0.15$) powder samples are listed in Table 6. Photographs of the samples are also shown in Figure 9. Although there was no regular change in brightness, the redness (a^*), yellowness (b^*), and chroma (C) values showed an increasing trend with the Ga^{3+}

doping. As the Ga^{3+} content increased, the color of the samples gradually changed to reddish black; among the samples listed in Table 6, the darkest black color was obtained for $Y(Mn_{0.85}Ga_{0.15})_2O_5$. As discussed in Figure 8, substituting some of the Mn^{3+} with Ga^{3+} increased the optical reflection in the near-infrared region (700–2500 nm), resulting in the increased *R* value. Among the samples in Table 6, $Y(Mn_{0.85}Ga_{0.15})_2O_5$ showed the highest *R* value (47.6%). This sample is considered to be the best black pigment with good NIR reflectance properties.

Table 6. Color coordinates and NIR solar reflectance (*R*) of the $Y(Mn_{1-x}Ga_x)_2O_5$ ($0 \leq x \leq 0.15$) powder samples.

Sample	*L**	*a**	*b**	*C*	*R*
YMn_2O_5	28.2	+2.83	−0.44	2.86	42.9
$Y(Mn_{0.95}Ga_{0.05})_2O_5$	25.8	+3.93	+0.53	3.97	43.7
$Y(Mn_{0.90}Ga_{0.10})_2O_5$	27.0	+4.30	+0.74	4.36	45.4
$Y(Mn_{0.85}Ga_{0.15})_2O_5$	25.8	+4.82	+1.25	4.98	47.6

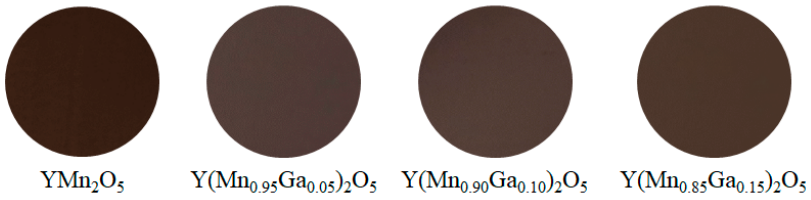

Figure 9. Photographs of the $Y(Mn_{1-x}Ga_x)_2O_5$ ($0 \leq x \leq 0.15$) samples.

The color coordinate data for the $Y(Mn_{0.85}Ga_{0.15})_2O_5$ sample in this study were compared with those of $YMnO_3$ and commercially available NIR-reflective black pigments such as Black 6350 (iron and chromium oxide; Asahi Kasei), Black 6301 (manganese and bismuth oxide, Asahi Kasei), and MPT-370 (calcium, manganese, and titanium oxide, Ishihara Sangyo), as shown in Table 7. Photographs of these pigments are also displayed in Figure 10.

Table 7. Color coordinates and NIR solar reflectance (*R*) of various black pigments.

Sample	*L**	*a**	*b**	*C*	*R*
$Y(Mn_{0.85}Ga_{0.15})_2O_5$	25.8	+4.82	+1.25	4.98	47.6
$YMnO_3$	22.6	−2.17	−9.04	9.30	43.9
Black 6350	25.3	+1.20	+4.06	4.23	41.3
Black 6301	23.7	+0.43	+1.05	1.13	38.7
MPT-370	23.0	+0.67	−0.27	0.72	44.0

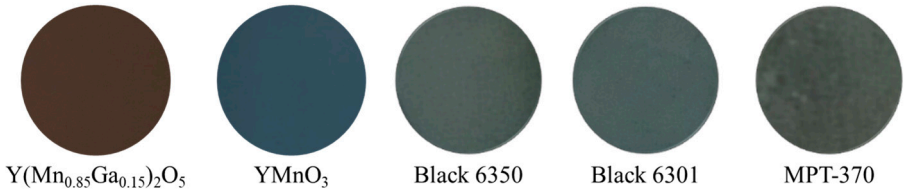

Figure 10. Photographs of $Y(Mn_{0.85}Ga_{0.15})_2O_5$, $YMnO_3$, Black 6350, Black 6301, and MPT-370 pellets made from powder samples.

The $Y(Mn_{0.85}Ga_{0.15})_2O_5$ sample synthesized in this study exhibited a reddish black color with a redness (a^*) value higher than those of $YMnO_3$ and the commercial products, indicating that its black color was inferior. However, $Y(Mn_{0.85}Ga_{0.15})_2O_5$ has high near-infrared reflectance, and its solar reflectance is higher than that of $YMnO_3$ and the commercial products, indicating that it has sufficient performance as a thermal barrier pigment.

3.3.4. Chemical Stability Test

The chemical stability of $Y(Mn_{0.85}Ga_{0.15})_2O_5$ was evaluated using powder samples. The powder samples were soaked in 4% CH_3COOH and 4% NH_4HCO_3 aqueous solutions, assuming vinegar and baking soda. After 24 h at room temperature, they were washed with deionized water and ethanol. The samples were then dried at room temperature. The color coordinate data of the samples after the chemical stability tests are summarized in Table 8, and photographs of the samples are also shown in Figure 11. The color tone and NIR solar reflectance changed slightly after the leaching tests in acid and base solutions. Although the $Y(Mn_{0.85}Ga_{0.15})_2O_5$ pigment was slightly less chemically stable, the *R* value of the sample still remained as high as those of commercial pigments.

Table 8. Color coordinate data of $Y(Mn_{0.85}Ga_{0.15})_2O_5$ samples before and after the chemical stability test.

Treatment	*L**	*a**	*b**	*C*	*R*
As synthesized	25.8	+4.82	+1.25	4.98	47.6
4% CH_3COOH	25.2	+4.39	+1.07	4.52	42.8
4% NH_4HCO_3	24.3	+4.49	−1.20	4.65	42.2

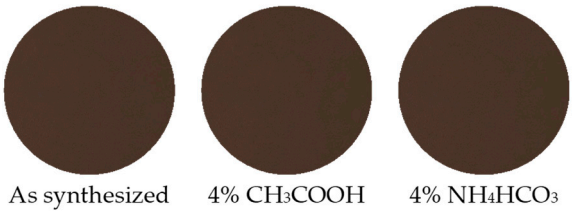

Figure 11. Photographs of $Y(Mn_{0.85}Ga_{0.15})_2O_5$ samples before and after the chemical stability test.

4. Conclusions

$Y(Mn_{1-x}Ga_x)_2O_5$ ($0 \leq x \leq 0.20$) samples were synthesized as environmentally benign inorganic NIR-reflective black pigments. In the *x* range from 0 to 0.15, the samples were obtained in a single phase and the lattice volume decreased linearly. These results indicate that solid solutions were successfully obtained in this *x* region. The $Y(Mn_{1-x}Ga_x)_2O_5$ ($0 \leq x \leq 0.15$) samples exhibited optical absorption in the visible light region due to the charge transfer transition between O^{2-} and Mn^{3+} and were reddish black in color. Among the synthesized samples, $Y(Mn_{0.85}Ga_{0.15})_2O_5$ showed the highest NIR reflectance (47.6%), which was also higher than that of conventional black pigments. In particular, this pigment exhibited higher solar reflectance in the wavelength range of 700–1300 nm, which is most involved in heat generation. Therefore, the $Y(Mn_{0.85}Ga_{0.15})_2O_5$ pigment will provide cooler roofs and exteriors for applications such as energy conservation buildings, as compared with the case of using conventional black pigments. The chemical stability of this sample is sufficient, and it has the potential to become a new NIR-reflective inorganic black pigment.

Author Contributions: The following are the author contributions to this study: Conceptualization, T.M. (Toshiyuki Masui); methodology, K.Y., T.M. (Takuro Morimoto), and T.M. (Toshiyuki Masui); validation, K.Y. and T.M. (Toshiyuki Masui); investigation, K.Y., S.M, and Y.N.; data curation, K.Y, S.M., Y.N., and T.M. (Takuro Morimoto); writing—original draft preparation, K.Y.; writing—review and editing, T.M. (Toshiyuki Masui); supervision, T.M. (Toshiyuki Masui); funding acquisition, T.M. (Toshiyuki Masui). All authors have read and agreed to the published version of the manuscript.

Funding: This research was funded by JSPS KAKENHI, grant numbers JP22K04698 and JP20H02439.

Institutional Review Board Statement: Not applicable.

Informed Consent Statement: Not applicable.

Data Availability Statement: Data are contained within the article.

Conflicts of Interest: The authors declare no conflict of interest.

References

1. Faulkner, E.B.; Schwartz, R.J. *High Performance Pigments*, 2nd ed.; Wiley-VCH: Weinheim, Germany, 2009.
2. Oka, R.; Masui, T. Synthesis and characterization of black pigments based on calcium manganese oxides for high near-infrared (NIR) reflectance. *RSC Adv.* **2016**, *6*, 90952–90957. [CrossRef]
3. Oka, R.; Iwasaki, S.; Masui, T. Improvement of near-infrared (NIR) reflectivity and black color tone by doping Zn^{2+} into the $Ca_2Mn_{0.85}Ti_{0.15}O_4$ structure. *RSC Adv.* **2019**, *9*, 38822–38827. [CrossRef]
4. Oka, R.; Hayakawa, T. Raman spectroscopic investigation and electronic state calculation for $Ca_2(Mn,Ti)O_4$ black pigments with high near-Infrared (NIR) reflectivity. *Inorg. Chem.* **2022**, *61*, 6500–6507. [CrossRef] [PubMed]
5. Morimoto, T.; Oka, R.; Minagawa, K.; Masui, T. Novel near-infrared reflective black inorganic pigment based on cerium vanadate. *RSC Adv.* **2022**, *12*, 16570–16575. [CrossRef]
6. Alonso, J.A.; Casais, M.T.; Martínez-Lope, M.J.; Martínez, J.L.; Ferandez-Díaz, M.T. A structural study from neutron diffraction data and magnetic properties of RMn_2O_5 (R = La, rare earth). *J. Phys. Condens. Matter* **1997**, *9*, 8515–8526. [CrossRef]
7. Kagomiya, I.; Kakimoto, K.; Ohsato, H. Precursor phenomenon on ferroelectric transition in multiferroic YMn_2O_5. *J. Eur. Ceram. Soc.* **2010**, *30*, 255–258. [CrossRef]
8. Yin, C.; Xia, Q.; Zhou, J.; Li, B.; Guo, Y.; Khan, A.; Li, X.; Xu, A. Direct electron transfer process-based peroxymonosulfate activation via surface labile oxygen over mullite oxide YMn_2O_5 for effective removal of bisphenol A. *Sep. Purif. Technol.* **2022**, *280*, 119924. [CrossRef]
9. Zhang, T.; Li, H.; Ynag, Z.; Cao, F.; Chen, H.; Liu, H.; Xiong, K.; Wu, J.; Hong, Z.; Wnag, W. Electrospun YMn_2O_5 nanofibers: A highly catalytic activity for NO oxidation. *Appl. Catal. B Environ.* **2019**, *247*, 133–141. [CrossRef]
10. Han, T.-C.; Lin, J.G. Enhancement of magnetic moment in Ca-doped helimagnetic YMn_2O_5. *J. Magn. Magn. Mater.* **2006**, *304*, e424–e426. [CrossRef]
11. Kim, J.-H.; Lee, S.-H.; Park, S.I.; Kenzelmann, M.; Harris, A.B.; Schefer, J.; Chung, J.-H.; Majkrzak, C.F.; Takeda, M.; Wakimoto, S.; et al. Spiral spin structures and origin of the magnetoelectric coupling in YMn_2O_5. *Phys. Rev. B* **2008**, *78*, 245115. [CrossRef]
12. Han, A.; Zhao, M.; Ye, M.; Liao, J.; Zhang, Z.; Li, N. Crystal structure and optical properties of $YMnO_3$ compound with high near-infrared reflectance. *Sol. Energy* **2013**, *91*, 32–36. [CrossRef]
13. Chen, Y.; Ma, Y.; Wang, Z.; Wang, X.; Liu, H.; Cheng, G.J. Molten salt synthesis of $YMnO_3$ powder with high near-infrared reflectivity. *Mater. Lett.* **2018**, *229*, 171–173. [CrossRef]
14. Chen, Z.; Xiao, R.-J.; Ma, C.; Qin, Y.-B.; Shi, H.-L.; Wang, Z.-W.; Song, Y.-J.; Wang, Z.; Tian, H.-F.; Yang, H.-X.; et al. Electronic structure of YMn_2O_5 studied by EELS and first-principles calculations. *Front. Phys.* **2012**, *7*, 429–434. [CrossRef]
15. Raj, A.K.V.; Rao, P.P.; Sameera, S.; Divya, S. Pigments based on terbium-doped yttrium cerate with high NIR reflectance for cool roof and surface coating applications. *Dyes Pigm.* **2015**, *122*, 116–125. [CrossRef]
16. Shannon, R.D. Revised effective ionic radii and systematic studies of interatomic distances in halides and chalcogenides. *Acta Cryst. A* **1976**, *32*, 751–767. [CrossRef]
17. Tamilarasan, S.; Laha, S.; Natarajan, S.; Gopalakrishnan, J. Li_2MnO_3: A Rare Red-Coloured Manganese (IV) Oxide Exhibiting Tunable Red−Yellow−Green Emission. *J. Mater. Chem. C* **2015**, *3*, 4794–4800. [CrossRef]
18. Kovaleva, N.N.; Gavartin, J.L.; Shluger, A.L.; Boris, A.V.; Stoneham, A.M. Lattice relaxation and charge-transfer optical transitions due to self-trapped holes in nonstoichiometric $LaMnO_3$ crystal. *J. Exp. Theor. Phys.* **2002**, *94*, 178–190. [CrossRef]
19. Kim, T.G.; Kim, S.J.; Lin, C.C.; Liu, R.S.; Chan, T.S.; Im, S.J. Melilite-type blue chromophores based on Mn^{3+} in a trigonal-bipyramidal coordination induced by interstitial oxygen. *J. Mater. Chem. C* **2013**, *1*, 5843–5848. [CrossRef]
20. Wang, D.; Su, D.; Zhong, M. Chromatic and near-infrared reflective properties of Fe^{3+} doped $KZnPO_4$. *Sol Energy* **2014**, *110*, 1–6. [CrossRef]

Disclaimer/Publisher's Note: The statements, opinions and data contained in all publications are solely those of the individual author(s) and contributor(s) and not of MDPI and/or the editor(s). MDPI and/or the editor(s) disclaim responsibility for any injury to people or property resulting from any ideas, methods, instructions or products referred to in the content.